

SiC-based Bidirectional Three-phase CLLC Resonant Converter with Integrated Magnetics for High-Power On-Board Charger Applications

Yunqi Chen

*EV Power Supply Design Department
Navitas Shanghai Design Center
Shanghai, China
yunqi.chen@navitassemi.com*

Minli Jia

*EV Power Supply Design Department
Navitas Shanghai Design Center
Shanghai, China
minli.jia@navitassemi.com*

Hao Sun

*EV Power Supply Design Department
Navitas Shanghai Design Center
Shanghai, China
hao.sun@navitassemi.com*

Jinlong Chen

*EV Power Supply Design Department
Navitas Shanghai Design Center
Shanghai, China
jinlong.chen@navitassemi.com*

Haisong Zhang

*EV Power Supply Design Department
Navitas Shanghai Design Center
Shanghai, China
hanson.zhang@navitassemi.com*

Zhen zhou

*EV Power Supply Design Department
Navitas Shanghai Design Center
Shanghai, China
zhen.zhou@navitassemi.com*

Abstract—Conventional full-bridge and half-bridge LLC resonant converters are no longer able to meet the growing power rating requirements and bi-directional operation needs of today's on-board chargers. By placing symmetrical resonant tanks on the secondary side of the transformer, The CLLC resonant converter enables bi-directional power flow while achieving a wide voltage gain range. In addition, the three-phase CLLC structure has the advantage of increasing the output power and decreasing current ripple. However, magnetic integration techniques must be employed to mitigate the increase in size and cost associated with additional magnetic components. In this paper, a symmetrical three-phase CLLC DC/DC resonant converter using an integrated transformer is presented and the gain characteristics of the converter are evaluated and analyzed. Finally, a 20 kW DC/DC converter prototype using SiC MOSFETs is built and the feasibility of the theoretical analysis is verified.

Index Terms—SiC MOSFET, DC/DC Resonant Converter, On Board Charger, Integrated Magnetics, Bidirectional Operation

I. INTRODUCTION

With the rapid expansion of the electric vehicle (EV) and plug-in hybrid electric vehicle (PHEV) markets, the development of on-board charger module (OBCM) technology is also gaining widespread attention. Several emerging OBCM technology trends can be summarized as follows. First, functions such as vehicle-to-vehicle (V2V), vehicle-to-grid (V2G), and vehicle-to-load (V2L), which are realized by EV battery discharge, have become popular [1], [2], so the mainstream market has been gradually occupied by bi-directional OBCMs with integrated discharge functions. Second, to meet charging scenarios under different power grids around the world, OBCMs compatible with single-phase AC grids and three-phase AC grids are preferred. On the other hand, compatibility

with three-phase AC grid charging is also necessary to support charging power rating up to 20 kW. The commonly accepted bidirectional three-phase AC/DC converter topology today requires the DC side to support 800 V bus voltage system, which means that commercially available silicon-based MOSFETs with a maximum breakdown voltage of 900 V are no longer suitable, while silicon-based IGBTs are limited in switching frequency [3], [4]. As a result, 1200 V SiC MOSFETs are the most favorable candidates benefiting from their high breakdown voltage and low switching losses. Finally, weight and size reduction is particularly important in automotive power applications since more compact systems lead to lower costs. Thus, many researches on OBCMs have focused on achieving higher power density by reducing the number of switching devices, increasing the switching frequency and introducing magnetic integration.

A typical OBCM consists of an AC/DC converter acting as a power factor corrector (PFC) and an isolated DC/DC converter to provide galvanic isolation. In the past, LLC resonant converters have been widely adopted in OBCM DC/DC stage due to their inherent excellent characteristics: zero voltage switching (ZVS) over the full load range, zero current switching (ZCS) for synchronous rectifiers and wide voltage gain range [5]–[7]. However, conventional full-bridge and half-bridge LLC converters have limited power ratings and are no longer able to meet the increasing power demands of OBCM applications [8]. In addition, the voltage gain less than unity in the reverse direction makes it unsuitable for bi-directional designs [9]. By placing an additional set of symmetrical resonant inductor and capacitor on the secondary side, the CLLC converter can achieve the same voltage gain range in reverse operation as in forward operation. Furthermore, by integrating three half-bridge CLLC converters, the

three-phase CLLLC resonant converter distributes the power equally among the three resonant tanks, so that higher power ratings can be realized [10]–[12]. Due to the 120° phase difference between the three synchronous rectifier outputs, the frequency of the three-phase CLLLC converter output ripple is six times the switching frequency [13]. Compared to the full-bridge LLC output with twice the switching frequency ripple, the lower ripple current reduces the size of the filter capacitor on the output side, allowing the system power density to be increased. The two options for connecting a three-phase CLLLC transformer are classified as being the Y-connection and the delta-connection, which have been studied and compared in [14]. The choice of these two connections is a trade-off between transformer winding losses and core losses. The Y-connection reduces the transformer winding voltage to two-thirds of the input voltage and is therefore preferred for OBCM applications using 800 V bus voltages [15].

Despite the significant advantages of three-phase CLLLC, three transformers and six resonant inductors are required, which considerably increases the system cost and size [16]. In this paper, a novel three-phase integrated transformer is proposed and designed. The three-phase windings are assembled onto a single core, which reduces core losses and size through flux cancellation. In addition to the three-phase integration, the proposed transformer is further integrated by employing the leakage inductance as resonant inductor. The desired leakage inductance can be obtained through loose coupling between primary and secondary windings.

II. ANALYSIS OF BIDIRECTIONAL THREE-PHASE CLLLC DC/DC CONVERTER

A. Gain Characteristics Analysis

The topology of bidirectional three-phase CLLLC DC/DC converter is shown in Fig. 1. Since the leakage inductance of the proposed integrated transformer is used as both primary and secondary resonant inductors and the leakage inductance is intrinsically distributed uniformly on both sides of the transformer, the relationship between the primary resonant inductor L_p and secondary resonant inductor L_s can be described as:

$$L_p = N^2 L_s \quad (1)$$

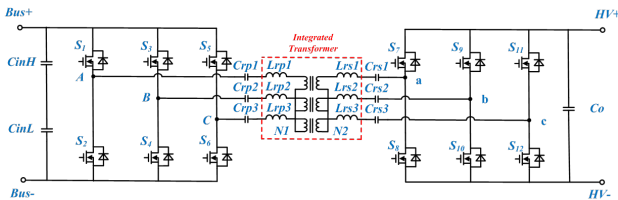


Fig. 1. Three phase CLLLC converter

Where $N = N_p/N_s$ is the turns ratio of the transformer. In order to simplify the design and maintain the consistency of the bi-directional operation of the converter. The resonant

capacitors on both sides of the proposed converter is also designed symmetrically:

$$C_s = N^2 C_p \quad (2)$$

By assuming that the energy is carried and transmitted only by the fundamental component of the switching frequency, the analysis of the gain characteristics of the resonant converter can be simplified by means of the fundamental harmonic approximation (FHA). Considering that each phase of the three-phase CLLLC converter has the identical resonant parameters and structure, only a single phase FHA analysis is required to obtain its gain characteristics. The equivalent single phase FHA circuit model of the three-phase CLLLC DC/DC converter is illustrated in Fig. 2. The transfer function of the FHA simplified circuit can be represented as:

$$H(j\omega) = \frac{R_{eq}}{R_{eq} + Z_s} \times \frac{(R_{eq} + Z_s) \parallel Z_m}{(R_{eq} + Z_s) \parallel Z_m + Z_p} \quad (3)$$

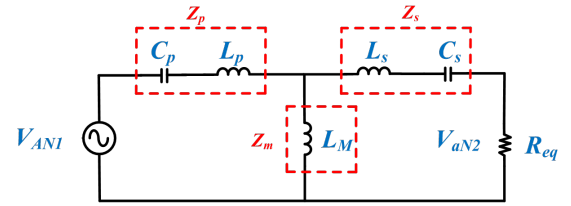


Fig. 2. Equivalent single phase FHA circuit of three-phase CLLLC converter

Since the power transmitted in each phase is one third of the total output power in a three-phase structure, the relationship between the output impedance R_o and the equivalent load R_{eq} coupled to the primary side can be expressed as:

$$\frac{1}{3} \cdot \frac{V_o^2}{R_o} = \frac{V_{aN2, RMS}^2}{R_{eq}} \quad (4)$$

The input voltage waveforms of the three resonant tanks are given in Fig. 3. Since the phase difference of the drive signal for each leg is 120° , the phase difference of the input voltage for each phase is also 120° . The fundamental component of the secondary midpoint-to-neutral voltage is reflected to the primary side:

$$V_{aN2}(t) = \frac{2N}{\pi} V_o \sin(\omega t) \quad (5)$$

From 4 and 5, the equivalent load R_{eq} coupled to the primary side in FHA circuit can be written as:

$$R_{eq} = \frac{6N^2}{\pi^2} \cdot R_o \quad (6)$$

To simplify the gain equation, the following definitions are given:

$$\omega_p = 1/\sqrt{L_p C_p} \quad (7)$$

$$\omega_n = \omega_s/\omega_p \quad (8)$$

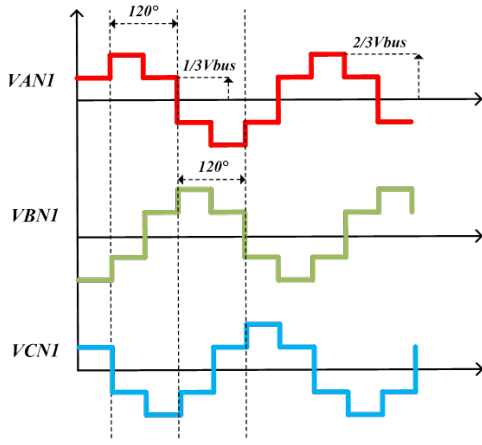


Fig. 3. Input voltage waveforms of 3-phase resonant tanks

$$Q = \sqrt{(L_P/C_P)/R_{eq}} \quad (9)$$

Where L_P and C_P are the primary resonant inductance and resonant capacitance, respectively. ω_p is the primary side resonant angular frequency. ω_n is the normalized resonant angular frequency. Q is the quality factor.

Thus the gain of the three-phase CLLLC resonant converter can be written as:

$$\frac{1}{\sqrt{\left(1 + \frac{1}{k} - \frac{1}{k\omega_n}\right)^2 + \left(\frac{Q}{k}\right)^2 \left[\left(k + \frac{k+1}{N^2}\right)\omega_n - \left(k + \frac{k+2}{N^2}\right)\frac{1}{\omega_n} + \frac{1}{N^2\omega_n^3} \right]^2}} \quad (10)$$

Combining 6 and 10, the normalized gain curves of the three-phase CLLLC can be plotted, as shown in Figs. 4 and 5. A proper DC/DC resonant converter design should ensure that the gain range is wide enough while the operating frequency shift is smooth.

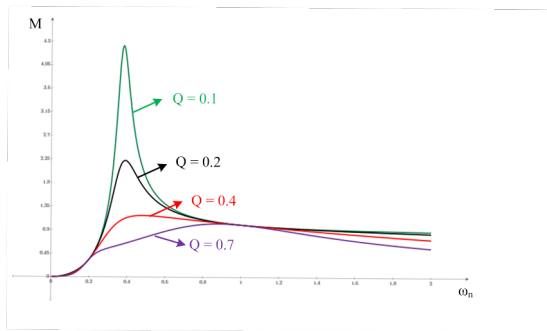


Fig. 4. The normalized gain curves with respect to Q ($k = 6$)

B. Design Steps of Resonant Parameters

Once the desired resonant frequency f_r and input and output voltage ranges of the three-phase CLLLC resonant converter are given, the design of the key parameters of the converter can be summarized in the following steps.

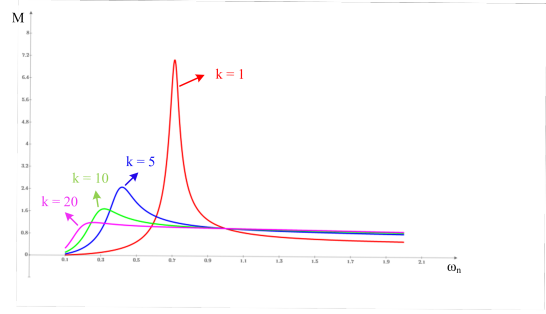


Fig. 5. The normalized gain curves with respect to k ($Q = 0.2$)

Step 1: Determine maximum operating voltage V_{Cr_pp} of the resonant capacitors. In order to maintain a sufficient safety margin, generally 80% of the rated voltage of the resonant capacitor is selected as its peak operating voltage. For example, a capacitor with a rated voltage of 630 V is designed with a peak operating voltage of 504 V.

Step 2: As the lowest voltage output point is designed to operate in quasi-resonant state to increase efficiency, the transformer turns ratio can be initially determined from the minimum input voltage V_{in_min} and minimum output voltage V_{out_min} :

$$N = \frac{V_{in_min}}{V_{out_min}} \quad (11)$$

The maximum resonant capacitor voltage stress occurs at the lowest output voltage point. Thus the resonant capacitance can be calculated by charge conservation in the quasi-resonant state:

$$C_p = \frac{1}{N} \cdot \frac{I_{o_max}}{V_{Cr_pp}} \times \frac{1}{2f_r} \quad (12)$$

where I_{o_max} is the average output current for full load operation at the lowest voltage output point.

Step 3: The resonant inductance L_p can be calculated from the desired resonant frequency as well as the resonant capacitance that has been determined in step 2:

$$L_p = \frac{1}{(2\pi f_r)^2 \cdot C_p} \quad (13)$$

Step 4: An excitation inductance L_M that is too small will lead to an increase in the conduction loss. On the other hand, the excitation current needs to provide enough energy to discharge the parasitic capacitance of the switching device during the dead time to ensure that the ZVS can be realized, its upper limit can be given as:

$$L_M \leq \frac{t_{dead}}{8C_j f_r} \quad (14)$$

Where t_{dead} is the dead time and C_j is the parasitic capacitance of the switching device. In addition, In engineering design, the value of $k = L_M/L_P$ is generally set between 5 and 10 to ensure that sufficient voltage gain can be provided at high voltage full load outputs.

III. DESIGN OF PROPOSED INTEGRATED TRANSFORMER

A. Transformer Structure and Leakage Inductance Design

The structure of the proposed integrated three-phase CLLC transformer is illustrated in Fig. 6. The primary side windings are distributed on both sides of the core and the secondary side windings are placed in the middle. Each phase is wound in the same way.

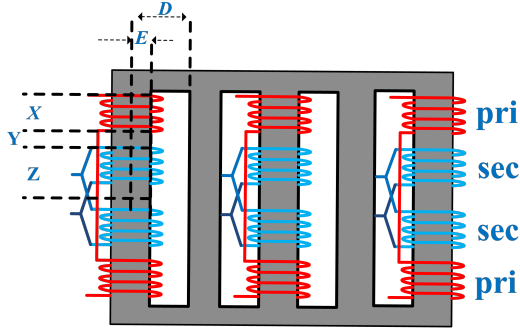


Fig. 6. Structure of integrated three-phase CLLC transformer

Employing the leakage inductance L_k of a transformer as the resonant inductor of an LLC type resonant converter has become a commonly accepted approach of magnetic integration. In the proposed integrated transformer, the coupling coefficient can be adjusted by varying the distance between the primary and secondary coils and thus L_k can be adjusted. The equation for calculating the leakage inductance has been derived in [9]. Based on the gaps defined in Fig. 6, the leakage inductance L_k of each phase can be expressed as:

$$L_k = \frac{2N_p^2 A_e \mu_o}{(D - E)^2} \cdot \left(\frac{X}{3} + Y + \frac{Z}{3} \right) \quad (15)$$

Where μ_o is the vacuum magnetic permeability and A_e is the effective cross-sectional area of the core center leg. When the number of transformer turns and core shape have been determined, L_k is positively related to the distance between the primary and secondary coils, and only the value of Y needs to be adjusted to obtain the desired leakage inductance. The simplified magnetic circuit model of the proposed integrated transformer is shown in Fig. 7. Ideally, there is a phase difference of 120° between the three phases and the sum of the fluxes of the three phases is equal to 0. In order to provide a decoupling path in case of three-phase unbalance, two legs without mounted coils are added to the proposed transformer. 3D Finite Element Analysis (FEA) simulations are carried out to validate the design, The maximum flux density distribution of the transformer core is captured and shown in Fig. 8. The center leg has a maximum magnetic flux density of 0.151 Tesla.

B. Effect of Unbalanced Three-phase Leakage Inductance

Unlike the three-phase CLLC resonant converter with delta-connected structure, the Y-connected structure cannot

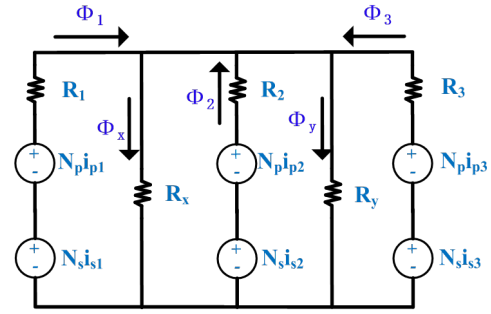


Fig. 7. Simplified magnetic circuit model of the proposed transformer

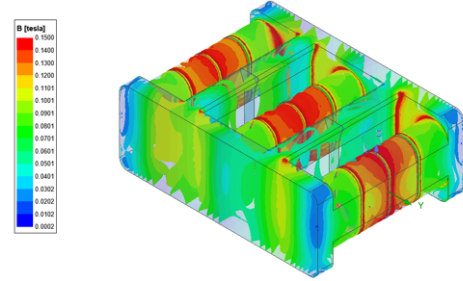
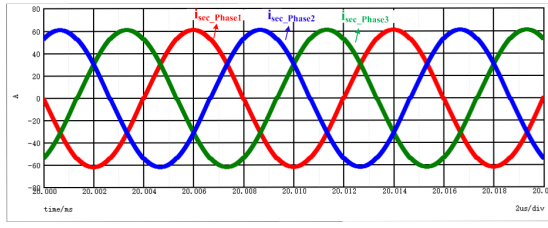


Fig. 8. FEA simulation result of the integrated three-phase transformer

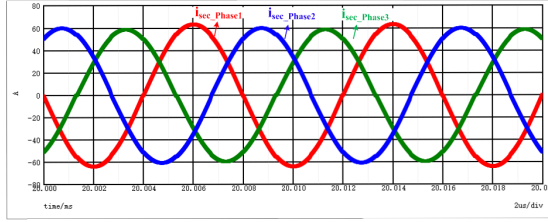
force the resonant currents through each phase to be equal. Especially when there is a serious imbalance in the resonant network, the current in one of the three-phase resonant tanks can far exceed that in the other two phases, resulting in an uneven distribution of thermal and device stresses among the three phases, and the output current ripple will be increased. Although several solutions to this problem have been given in [13], [17]. However, the needs for the addition of extra sampling circuits or complex control algorithms could lead to increased costs and reduced reliability.

As can be seen in Fig. 6, the three-phase structure of the proposed integrated transformer is not identical. The two phases distributed on both sides have a symmetrical structure therefore their leakage inductances are equal. However, the phase in the center is surrounded by the two ferrite legs with higher permeability than μ_o , which makes it has an inherently larger leakage inductance compared to the other two phases if the same winding gaps are applied. To find out the effect of unbalanced leakage inductance on the three-phase resonant current, the circuit simulation under different levels of leakage inductance imbalance is carried out and the simulation results are shown in Fig. 9. A 30% deviation in leakage inductance can cause a difference in the three-phase resonant RMS current of more than 5 A.

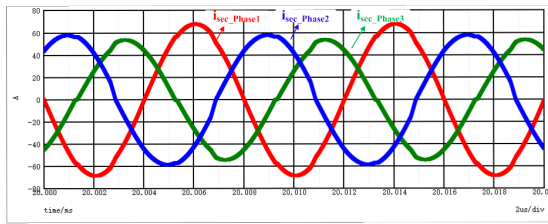
Benefiting from the fact that the leakage inductance of the proposed integrated transformer can be adjusted by the spacing between windings, only a slight increase in the winding gap of the middle phase is required to solve the aforementioned problem. The precise leakage inductance value can be obtained by FEA simulation. Without the introduction of additional



(a) $L_{k_center} = L_{k_side}$



(b) $L_{k_center} = 1.1 \cdot L_{k_side}$



(c) $L_{k_center} = 1.3 \cdot L_{k_side}$

Fig. 9. Effect of unbalanced leakage inductance on the secondary resonant current

control algorithms, the tolerance of the resonant network should be reasonably controlled within a certain range so that the current imbalance does not exceed an acceptable range.

IV. EXPERIMENT RESULT

To verify the feasibility of the above evaluations and analysis, a 20 kW bi-directional three-phase CLLC resonant converter prototype is constructed in the laboratory, which is shown in Fig. 10.

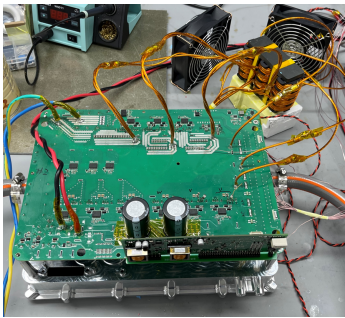


Fig. 10. 20 kW bi-directional three-phase CLLC resonant converter prototype

G3R40MT12K, a 1200 V automotive SiC MOSFET from GeneSiC Semiconductor, is selected as the switching device on the primary side of the prototype. The adoption of the

G3R40MT12K results in higher system efficiency and reliability due to its fast and efficient switching characteristics and lower temperature coefficient of on-state resistance. In addition, the use of the TO-247-4 package facilitates layout and thermal design. Key parameters of the G3R40MT12K are given in Table I.

Several key system specifications are shown in Table II. Using the design methodology mentioned in Section II, the key resonant parameters being designed are also summarized in Table II.

TABLE I
KEY PARAMETERS OF G3R40MT12K

| Parameter | | Value |
|---|---------------|--------|
| Drain-Source Voltage | $V_{DS(max)}$ | 1200 V |
| Continuous Forward Current | I_D | 55 A |
| Drain-Source On-State Resistance | $R_{DS(ON)}$ | 40 mΩ |
| Output Capacitance | C_{oss} | 88 pF |
| Total Gate Charge | Q_g | 88 nC |

TABLE II
RESONANT PARAMETERS AND SPECIFICATIONS

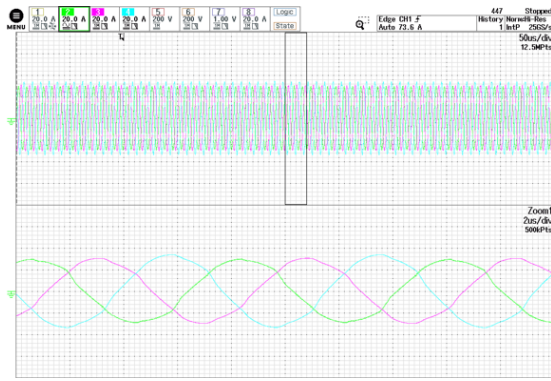
| Parameter | | Value |
|-------------------------------------|-------------------|--------------------|
| BUS Voltage | V_{in} | 660 Vdc to 840 Vdc |
| Full Load Battery Voltage | V_{out} | 330 Vdc to 500 Vdc |
| Maximum Charging Power | $P_{charging}$ | 20 kW |
| Maximum Discharging Power | $P_{discharging}$ | 15 kVA |
| Primary Resonant Inductance | L_P | 12 μH |
| Primary Resonant Capacitance | C_P | 130 nF |
| Excitation inductance | L_M | 70 μH |
| Resonant Frequency | f_r | 127 kHz |
| Primary number of turns | N_P | 28 |
| Secondary number of turns | N_S | 14 |

Fig. 11 shows the three-phase charging resonant current waveforms at the boundary output voltage points. Due to the inevitable tolerance in resonant capacitors and leakage inductance, it can still be observed from Fig. 11(a) that the three-phase resonant currents are not exactly equal at high current output. However, the difference in the three-phase currents is not enough to cause an over-stressing problem and thus is negligible.

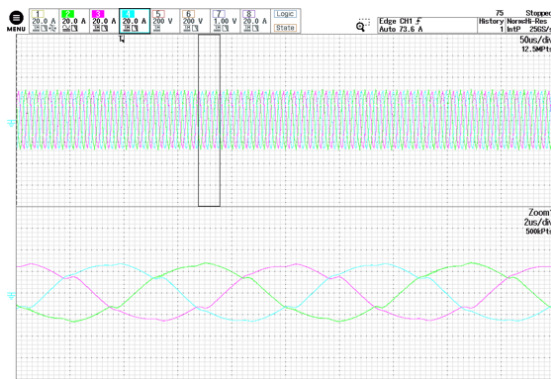
The charging and discharging efficiency of the prototype when operating at full load are demonstrated in Fig. 12. Most of the output voltage operating points are designed to operate in a quasi-resonant state as a way to achieve optimal system efficiency. A peak charging efficiency of 98.7% is achieved at the highest output voltage. Due to lower power requirements in the discharge direction, full range higher discharging efficiencies can be observed.

V. CONCLUSIONS

In this paper, a SiC-based three-phase CLLC bidirectional DC/DC converter with integrated transformer is presented. The proposed converter has the advantages of wide gain range, high power level and realizing bi-directional operation, which



(a) $V_{BAT} = 300 \text{ V}$, $f_s > f_{r1}$, 80% Load



(b) $V_{BAT} = 500 \text{ V}$, $f_s < f_{r1}$, Full Load

Fig. 11. Typical three-phase primary resonant current waveforms

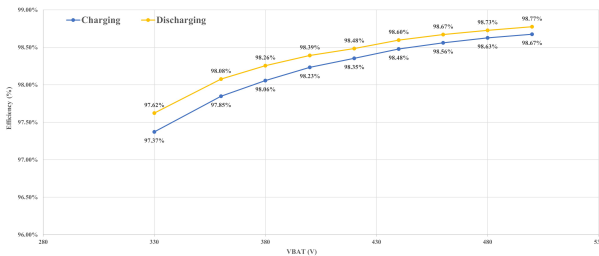


Fig. 12. Full load charging and discharging efficiency against battery voltage of the three-phase CLLC DC/DC converter

meets the development trend of on-board charger applications. A 20 kW prototype is built to verify the feasibility of the theoretical analysis. The full load charging peak efficiency of the prototype reaches 98.7%.

REFERENCES

- [1] X. Wang, Y. Liu, W. Qian, B. Wang, X. Lu, K. Zou, N. González-Santini, U. Karki, F. Z. Peng, and C. Chen, "A 25kW SiC Universal Power Converter Building Block for G2V, V2G, and V2L Applications," in *2018 IEEE International Power Electronics and Application Conference and Exposition (PEAC)*, 2018, pp. 1–6.
- [2] C. K. Gowda, V. G. Khedekar, N. Anandh, L. R. S. Paragond, and P. Kulkarni, "Bidirectional on-board EV battery charger with V2H application," in *2019 Innovations in Power and Advanced Computing Technologies (i-PACT)*, vol. 1, 2019, pp. 1–5.

- [3] P. M. Johnson and K. H. Bai, "A dual-DSP controlled SiC MOSFET based 96technology," in *2017 IEEE Symposium Series on Computational Intelligence (SSCI)*, 2017, pp. 1–5.
- [4] J. Shao, A. Barkley, Y. Hu, T. S. Ong, and B. Agrawal, "SiC MOSFET Based Bi-Directional 3-Phase AC/DC Converter," in *2018 IEEE Energy Conversion Congress and Exposition (ECCE)*, 2018, pp. 2890–2895.
- [5] B. Yang, F. Lee, A. Zhang, and G. Huang, "LLC resonant converter for front end DC/DC conversion," in *APEC. Seventeenth Annual IEEE Applied Power Electronics Conference and Exposition (Cat. No.02CH37335)*, vol. 2, 2002, pp. 1108–1112 vol.2.
- [6] Y. S. Dow, H. I. Son, and H.-D. Lee, "A study on Half bridge LLC resonant converter for battery charger on board," in *8th International Conference on Power Electronics - ECCE Asia*, 2011, pp. 2694–2698.
- [7] S. Hu, J. Deng, C. Mi, and M. Zhang, "LLC resonant converters for PHEV battery chargers," in *2013 Twenty-Eighth Annual IEEE Applied Power Electronics Conference and Exposition (APEC)*, 2013, pp. 3051–3054.
- [8] W. Martinez, M. Noah, S. Endo, K. Nanamori, S. Kimura, Y. Itoh, M. Yamamoto, J. Imaoka, and K. Umetani, "Three-phase LLC resonant converter with integrated magnetics," in *2016 IEEE Energy Conversion Congress and Exposition (ECCE)*, 2016, pp. 1–8.
- [9] G. Liu, D. Li, J. Q. Zhang, B. Hu, and M. L. Jia, "Bidirectional CLLC resonant DC-DC converter with integrated magnetic for OBCM application," in *2015 IEEE International Conference on Industrial Technology (ICIT)*, 2015, pp. 946–951.
- [10] W. H. Martinez and C. A. Cortes, "High power density interleaved DC-DC converter for a high performance electric vehicle," in *2013 Workshop on Power Electronics and Power Quality Applications (PEPQA)*, 2013, pp. 1–6.
- [11] M. Hirakawa, M. Nagano, Y. Watanabe, K. Ando, S. Nakatomi, S. Hashino, and T. Shimizu, "High power density interleaved DC/DC converter using a 3-phase integrated close-coupled inductor set aimed for electric vehicles," in *2010 IEEE Energy Conversion Congress and Exposition*, 2010, pp. 2451–2457.
- [12] W. Martinez, J. Imaoka, and M. Yamamoto, "Analysis of output capacitor voltage ripple of the three-phase transformer-linked boost converter," in *2015 17th European Conference on Power Electronics and Applications (EPE'15 ECCE-Europe)*, 2015, pp. 1–9.
- [13] H.-S. Kim, J.-W. Baek, M.-H. Ryu, J.-H. Kim, and J.-H. Jung, "The High-Efficiency Isolated AC-DC Converter Using the Three-Phase Interleaved LLC Resonant Converter Employing the Y-Connected Rectifier," *IEEE Transactions on Power Electronics*, vol. 29, no. 8, pp. 4017–4028, 2014.
- [14] C. Fei, R. Gadelrab, Q. Li, and F. C. Lee, "High-Frequency Three-Phase Interleaved LLC Resonant Converter With GaN Devices and Integrated Planar Magnetics," *IEEE Journal of Emerging and Selected Topics in Power Electronics*, vol. 7, no. 2, pp. 653–663, 2019.
- [15] N. A. Dung, H.-C. Hsieh, J.-Y. Lin, H.-J. Chiu, and J.-S. Lai, "Design of Bidirectional DC-DC Converter for Energy Storage System in High Power Application," in *2019 IEEE 4th International Future Energy Electronics Conference (IFEEC)*, 2019, pp. 1–4.
- [16] R. Gadelrab, F. C. Lee, and Q. Li, "Three-Phase Interleaved LLC Resonant Converter with Integrated Planar Magnetics for Telecom and Server Application," in *2020 IEEE Applied Power Electronics Conference and Exposition (APEC)*, 2020, pp. 512–519.
- [17] S. A. Arshadi, M. Ordonez, W. Eberle, M. A. Saket, M. Craciun, and C. Botting, "Unbalanced Three-Phase LLC Resonant Converters: Analysis and Trigonometric Current Balancing," *IEEE Transactions on Power Electronics*, vol. 34, no. 3, pp. 2025–2038, 2019.